ORGANIC CHEMISTRY FRONTIERS

RESEARCH ARTICLE

View Article Online
View Journal | View Issue

Cite this: *Org. Chem. Front.*, 2024, **11**, 3109

NBN/BNB-doped phenalenyl homo- and heterodyads: structural uniformity but optoelectronic diversity†

Alexander S. Scholz,[a] Thomas Froitzheim, *[b] Michael Bolte, [a] Hans-Wolfram Lerner, [a] Jan-M. Mewes [b] and Matthias Wagner *[a]

Phenalenyl anions and cations are fundamentally interesting but highly reactive complementary species. One way to tame this reactivity and prevent comproportionation as soon as the two species are allowed to interact is by switching to the isosteric NBN- or BNB-containing heterocycles. Herein, we show that the heteroatom-doped pair preserves to a certain extent the desirable complementarity of the original carbonaceous molecules. To this end, we synthesized a series of 1,4-phenylene-bridged $(NBN)_2$- or $(BNB)_2$-homodyads and (NBN,BNB)-heterodyads. The homodyads are accessible *via* treatment of a 1,4-diborylated benzene with a 1,8-diaminonaphthalene or of 1,4-diaminobenzene with 1,8-naphthalenediyl-bridged diborane(6), respectively. The heterodyads were prepared from the same diborane(6) and an NBN-phenalenyl with B-bonded *p*-NH_2-aryl substituent. All products were characterized by NMR spectroscopy, X-ray crystallography, cyclic voltammetry, UV/vis absorption and emission spectroscopy, as well as state-of-the-art quantum-chemical calculations. The heterodyads undergo both oxidation and reduction and thus qualify as ambipolar compounds. Any *intra*molecular NBN-to-BNB charge-transfer (CT) emission is negligible on conformational grounds. In contrast, an appreciable aggregation-induced green emission is achieved by adding H_2O to THF solutions of the heterodyads and is presumably caused by *inter*molecular CT between head-to-tail aligned molecules upon aggregation.

Received 12th March 2024,
Accepted 7th April 2024

DOI: 10.1039/d4qo00468j

rsc.li/frontiers-organic

Introduction

Polycyclic aromatic hydrocarbons (PAHs) are an important compound class for the development of novel organic optoelectronic materials.[1] One reason is that PAHs can be derivatized in various ways to generate a wide range of properties. A particularly powerful derivatization mode is the selective replacement of individual carbon atoms within the π-electron system by other p-block elements, especially boron and nitrogen ("B,N-doping" to obtain "B,N-PAHs").[2] Depending on the number and positioning of the dopant heteroatoms, the electronic structures of the resulting B,N-PAHs are influenced in different ways, while their molecular structures remain largely unchanged compared to those of the carbonaceous parent compounds.[3] With this in mind, we recently set out to prepare largely isostructural B,N-PAHs with complementary electron-donor and -acceptor characteristics. As parent scaffold, we selected the triangular (D_{3h}), odd-alternant hydrocarbon phenalenyl, which consists of three mutually annulated benzene rings and has a fully conjugated system of 13 π-electrons.[4] The neutral radical has a nonbonding molecular orbital and can therefore, in principle, undergo redox transitions to form an antagonistic anion/cation couple (Fig. 1, **I**/**II**).[5–7] Since an N or

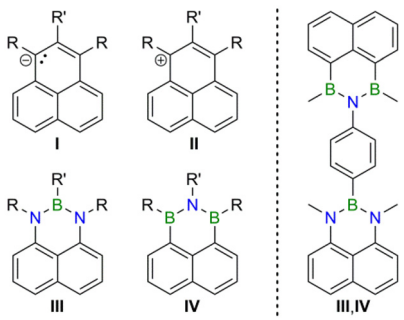

Fig. 1 Carbonaceous phenalenyl anions (**I**) and cations (**II**), their respective NBN- (**III**) and BNB-doped (**IV**) analogs, and the corresponding 1,4-phenylene-bridged donor–acceptor dyad (**III**,**IV**).

[a]*Institut für Anorganische und Analytische Chemie, Goethe-Universität Frankfurt am Main, Max-von-Laue-Straße 7, 60438 Frankfurt am Main, Germany. E-mail: matthias.wagner@chemie.uni-frankfurt.de*
[b]*Mulliken Center for Theoretical Chemistry, Institut für Physikalische und Theoretische Chemie, Rheinische Friedrich Wilhelms-Universität Bonn, Beringstr. 4, 53115 Bonn, Germany. E-mail: th.froitzheim@thch.uni-bonn.de*

†Electronic supplementary information (ESI) available: Experimental and computational details, analytical data. CCDC 2338779–2338788. For ESI and crystallographic data in CIF or other electronic format see DOI: **https://doi.org/10.1039/d4qo00468j**

B atom has one electron more or fewer, respectively, than a C atom, the NBN-doped phenalenyl **III**[8,9] can be considered a neutral equivalent of the phenalenyl anion, while the BNB-doped species **IV**[10,11] is an isoster of the phenalenyl cation (Fig. 1). In a previous publication, we have already shown that equimolar co-precipitates of **III**- and **IV**-type compounds can exhibit photoluminescence properties not seen in the individual components; a thorough quantum-chemical study revealed an intermolecular **III**-to-**IV** charge transfer (CT) as the origin of the observed aggregation-induced emission.[12] Herein, we now report the synthesis of **III**- and **IV**-based, 1,4-phenylene-bridged donor–donor (**III**,**III**), acceptor–acceptor (**IV**,**IV**), and donor–acceptor dyads (**III**,**IV**). We will show a truly ambipolar character of the donor–acceptor species and remarkably different optical properties of the three different kinds of dyads.

Results and discussion

To prove the claim that B,N-doping indeed provides access to structurally uniform but electronically diverse compounds, we prepared the series of $(NBN)_2$- ($\mathbf{1^{Me}}$), $(BNB)_2$- ($\mathbf{2^{Me}}$), and (NBN, BNB)-phenalenyls ($\mathbf{3^{Me,Me}}$, Scheme 1). Compound $\mathbf{1^{Me}}$ is accessible from 1,8-diaminonaphthalene **A** and the 1,4-diborylated benzene **B** *via* established coordination chemistry.[13] Aminolysis of 2 equiv. of the 1,8-naphthalenediyl-bridged diborane(6) **C** with 1 equiv. of 1,4-diaminobenzene **D** furnishes the parent $(BNB)_2$-phenalenyl $\mathbf{2^H}$, which can be converted to its derivatives $\mathbf{2^{Me}}$ and $\mathbf{2^{Mes}}$ by treatment with MeMgBr and MesMgBr (Mes = mesityl), respectively. This fourfold nucleophilic substitution reaction is remarkably straightforward considering that H^- ions act as the leaving groups. LiH elimination is key to the introduction of the 4-aminophenyl substituent into the NBN-phenalenyl **E** to give **5** or **6** (R′ = H, Me). After deprotection of the NH_2 group, the BNB functionality is again assembled *via* an aminolysis step. Reaction of the resulting BH intermediate with MeMgBr or MesMgBr affords the donor–acceptor dyads $\mathbf{3^{Me,Me}}$ and $\mathbf{3^{Me,Mes}}$, respectively. Compound $\mathbf{4^{Me,Mes}}$, which contains a sterically more demanding doubly methylated phenylene linker, was prepared in an analogous manner.

NMR-spectroscopic and crystallographic characterization

The ^{1}H NMR spectrum of the $(NBN)_2$-dyad $\mathbf{1^{Me}}$ shows one singlet for the NMe groups, two doublets as well as one virtual triplet for the 1,8-naphthalenediyl moieties, and one singlet for the four equivalent protons of the 1,4-phenylene bridge. A qualitatively similar spectrum is obtained for the $(BNB)_2$ compound $\mathbf{2^{Me}}$. The dyad $\mathbf{3^{Me,Me}}$ is characterized by the proton-signal patterns of the NBN- and BNB-phenalenyl moieties with equal integral values; the 1,4-phenylene protons give rise to an AA′BB′ spin system. The NMR spectra of all other products were also fully assigned and are consistent with the proposed molecular structures. With respect to electronic structure elucidation, the following feature from the $^{13}C\{^1H\}$ NMR spectra is particularly revealing: in all cases, the NBN-phenalenyl C-nuclei *ortho* and *para* to the N atoms are significantly better shielded than the corresponding C-nuclei within the BNB-phenalenyl fragments (*cf.* $\mathbf{1^{Me}}$: *o*-C: 103.8/120.7 ppm, *p*-C: 118.4 ppm *vs.* $\mathbf{2^{Me}}$: 138.2/136.9 ppm, 133.0 ppm). Given that the magnetic shielding of a C(sp^2) atom within a delocalized π-electron system increases with increasing electron density at this position,[14] NMR spectroscopy provides experimental support for the classification of NBN- and BNB-phenalenyls as electron donors and acceptors, respectively.

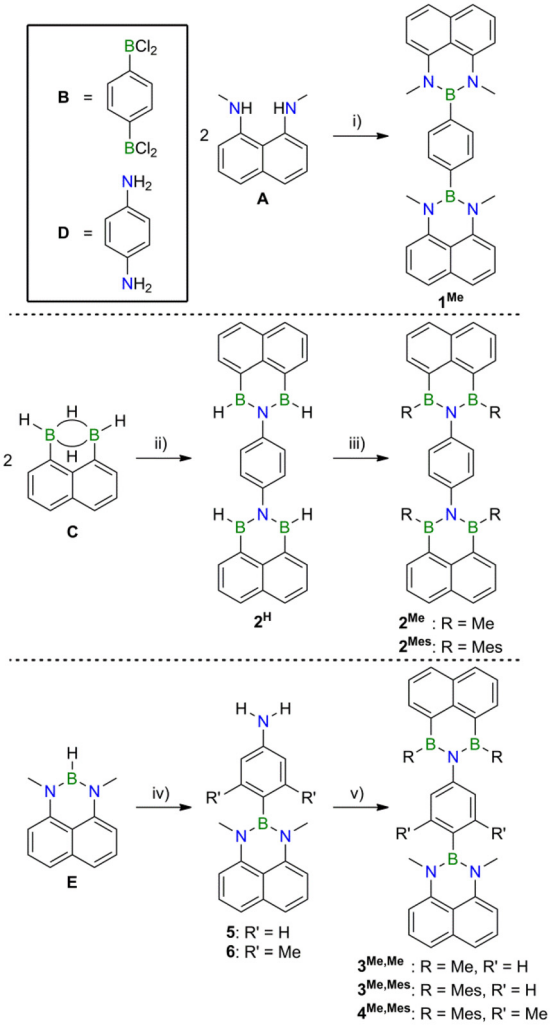

Scheme 1 Syntheses of compounds $\mathbf{1^{Me}}$–**6**. Reagents and conditions: (i) 1 equiv. of **B** and 4 equiv. of *i*-Pr_2NEt, toluene, −78 °C to room temperature; yield: 80%. (ii) 1 equiv. of **D**, CH_2Cl_2, heated under reflux; yield: 78%. (iii) R = Me: 4 equiv. of MeMgBr, Et_2O, 0 °C to room temperature; yield: 76%. R = Mes: 4.3 equiv. of MesMgBr, THF, −78 °C to room temperature; yield: 55%. (iv) R′ = H: 1. 1 equiv. of 4-$(Me_3Si)_2N$-C_6H_4-Li, THF, −78 °C to room temperature; 2. 1 vol% conc. aqueous HCl in MeOH, THF, room temperature; yield: 65%. R′ = Me: 1. 1 equiv. of 2,6-Me_2-4-$(Me_3Si)_2N$-C_6H_2-Li, THF, −78 °C to room temperature; 2. 1 vol% conc. aqueous HCl in MeOH, THF, room temperature; yield: 47%. (v) R = Me, R′ = H: 1. 1 equiv. of **C**, C_6H_6, room temperature; 2. 2.2 equiv. of MeMgBr, THF, 0 °C to room temperature; yield: 68%. R = Mes, R′ = H: 1 equiv. of **C**, C_6H_6, room temperature; 2. 2 equiv. of MesMgBr, THF, room temperature; yield: 75%. R = Mes, R′ = Me: 1 equiv. of **C**, C_6H_6, room temperature; 2. 2.3 equiv. of MesMgBr, THF, 0 °C to room temperature; yield: 53%.

The molecular structures of all products $\mathbf{1}^{\mathbf{Me}}\cdot CH_2Cl_2$, $\mathbf{2}^{\mathbf{H}}$, $\mathbf{2}^{\mathbf{Me}}\cdot CH_2Cl_2$, $\mathbf{2}^{\mathbf{Mes}}\cdot C_6H_{12}$, $\mathbf{3}^{\mathbf{Me,Me}}\cdot$THF, $\mathbf{3}^{\mathbf{Me,Mes}}\cdot C_6H_{14}$, and $\mathbf{4}^{\mathbf{Me,Mes}}$ were confirmed by X-ray crystallography (all solid-state structures, including **B**, **5**, and **6**, are shown in Fig. S56–S67†). We refrain from a detailed discussion of bond lengths and bond angles, as these are very similar to those of corresponding published heterocycles.[12] One result, however, is noteworthy: in the crystal lattice of $\mathbf{3}^{\mathbf{Me,Me}}\cdot$THF, the ambipolar mixed (NBN,BNB)-dyad is located on a crystallographic mirror plane, rendering the NBN and BNB halves of the molecules indistinguishable. We take this as confirmation of our basic claim that NBN- and BNB-phenalenyls have essentially identical molecular scaffolds despite their different electron-donor and -acceptor character. For an assessment of possible intramolecular charge-transfer (CT) interactions between the NBN- and BNB-phenalenyl residues (see below), one should also consider the dihedral angles between these heteroatomic units and the respective 1,4-phenylene bridges (C_6) in the ambipolar species $\mathbf{3}^{\mathbf{Me,Me}}$ (NBN//C_6 = BNB//C_6 = 77.60(6)°), $\mathbf{3}^{\mathbf{Me,Mes}}$ (NBN//C_6 = 62.82(11)°, BNB//C_6 = 62.58(10)°), and $\mathbf{4}^{\mathbf{Me,Mes}}$ (NBN//C_6 = 79.44(9)°, BNB//C_6 = 74.94(11)°). Although the molecular conformations in solution are likely different from those in the solid state (see the ESI† for a comparison to the calculated structures), it is safe to conclude that (i) dihedral angles in the range of 60°–80° are accessible and (ii) dihedral angles of about 80° are assumed both with and without bulky Me substituents at the 1,4-phenylene bridge (but will certainly be favored in the former case).

Optoelectronic properties

To gain further information about their electronic structures, the NBN- and BNB-phenalenyls were investigated by cyclic voltammetry (CV; [*n*-Bu_4N][PF_6], *vs.* FcH/FcH^+; Table 1). As expected, the NBN-containing species undergo electrochemical oxidation with peak potentials in the range of E_{pa} = 0.08 to 0.39 V, but in most cases the corresponding transitions are not (fully) reversible (Fig. 2a and S53–S54†). The BNB-containing congeners are electrochemically better behaved and undergo reduction at half-wave potentials of $E_{1/2}$ = −2.33 to −2.43 V. Of the $(BNB)_2$-dyads, $\mathbf{2}^{\mathbf{Me}}$ shows one reversible reduction event at $E_{1/2}$ = −2.43 V (Fig. S51†), while the more sterically protected $\mathbf{2}^{\mathbf{Mes}}$ gives rise to two barely resolved redox waves at approx. $E_{1/2}$ = −2.33 V (Fig. 2b). In any case, this points towards an only weak electronic communication between the two BNB-phenalenyl halves in $\mathbf{2}^{\mathbf{Mes}}$. In terms of electrochemistry, our best-performing compound is $\mathbf{4}^{\mathbf{Me,Mes}}$, as it undergoes both reversible oxidation ($E_{1/2}$ = 0.22 V) and reversible reduction ($E_{1/2}$ = −2.35 V, Fig. 2c).

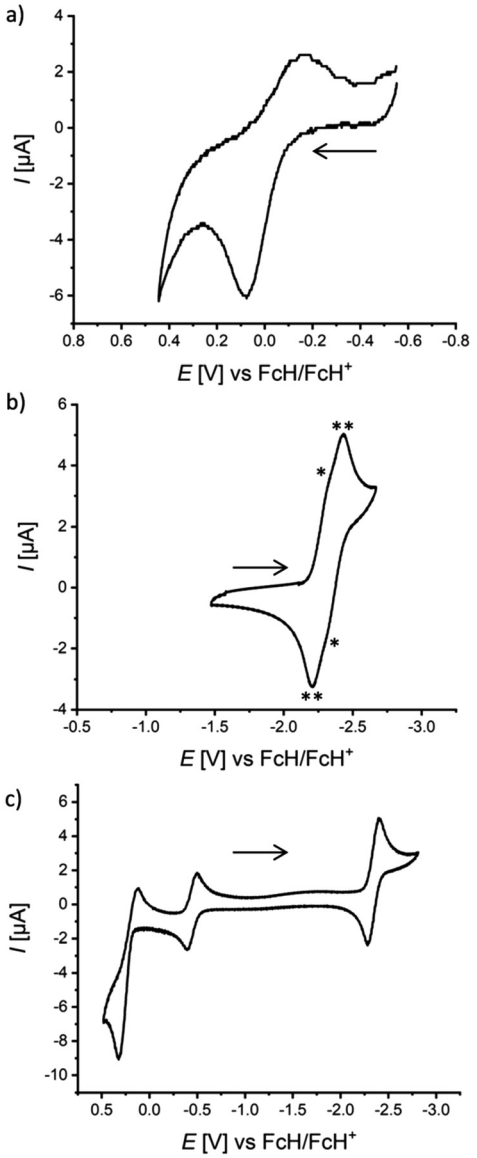

Fig. 2 Cyclic voltammograms of (a) $\mathbf{1}^{\mathbf{Me}}$, (b) $\mathbf{2}^{\mathbf{Mes}}$, and (c) $\mathbf{4}^{\mathbf{Me,Mes}}$ in THF (against the FcH/FcH^+ redox couple, room temperature, [*n*-Bu_4N][PF_6] (0.1 M), scan rate 200 mV s^{-1}). The cyclic voltammogram of $\mathbf{2}^{\mathbf{Mes}}$ in (b) shows two partly resolved reduction waves with very similar $E_{1/2}$ values (marked with "*" and "**"). The redox wave at −0.446 V in (c) corresponds to the Fc^*H/Fc^*H^+ redox couple (Fc*H: decamethylferrocene; internal standard).

Table 1 Selected electrochemical (THF) and photophysical data (C_6H_{12}) of compounds $\mathbf{1}^{\mathbf{Me}}$–$\mathbf{4}^{\mathbf{Me,Mes}}$. Experimental details and further data for each compound can be found in the ESI†

	$E_{1/2}$ [V]	E_{pa} [V]	E_{pc} [V]	λ_{abs} [b] [nm]	λ_{em} [d] [nm]	Φ_{PL} [e] [%]
$\mathbf{1}^{\mathbf{Me}}$	—	0.08	—	333[c]	—	—
$\mathbf{2}^{\mathbf{Me}}$	−2.43	—	−2.52	316[c]	371[c]	2[c]
$\mathbf{2}^{\mathbf{Mes}}$	*ca.* −2.33[a]	—	−2.43	342	434[c]	22[c]
$\mathbf{3}^{\mathbf{Me,Me}}$	−2.43	0.39	−2.55	332[c]	—	—
$\mathbf{3}^{\mathbf{Me,Mes}}$	−2.35	0.33	−2.47	327	395	6
$\mathbf{4}^{\mathbf{Me,Mes}}$	0.22, −2.35	0.32	−2.40	328	392	3

[a] The cyclic voltammogram of $\mathbf{2}^{\mathbf{Mes}}$ shows two partly resolved reduction waves with very similar $E_{1/2}$ values (*cf.* "*" and "**" in Fig. 2b). [b] Most intense maximum of each absorption spectrum in C_6H_{12}. [c] For solubility and/or comparability reasons, this measurement was performed in CH_2Cl_2. [d] In case of vibrationally structured emission bands (C_6H_{12}), the most intense maximum is given. λ_{ex} [nm] = 330 ($\mathbf{2}^{\mathbf{Me}}$), 335 ($\mathbf{2}^{\mathbf{Mes}}$), 327 ($\mathbf{3}^{\mathbf{Me,Mes}}$), and 328 ($\mathbf{4}^{\mathbf{Me,Mes}}$). [e] Quantum yields were determined by using a calibrated integrating sphere.

The electrochemical measurements align well with the computed adiabatic redox potentials at the ωB97X-D3/ma-def2-QZVPP/SMD[THF][15–22] level of theory for fully relaxed r^{2}SCAN-3c/SMD[THF][23] structures of the neutral, anionic, and cationic species (against the FcH/FcH$^+$ redox couple, see the ESI† for computational details):[47,48] for compounds containing the NBN-motif, theory predicts first oxidation potentials between 0.26 V and 0.37 V, while the first reduction potentials of the BNB-containing congeners range between −2.49 V and −2.69 V (see Table S15†). Deviations between the experimental and theoretical redox potentials therefore remain within 0.3 V, as is expected from the limitations of DFT and implicit solvation for radical and charged species.[20,24–26] The inspection of the highest occupied (HOMO) and lowest unoccupied molecular orbitals (LUMO) (see Fig. S88–S93†) confirms that electrochemical activity is primarily localized on the NBN- and BNB-phenalenyl units and to a much lesser extent on the 1,4-phenylene bridges. Although the heterocyclic moieties belonging to the same molecule appear largely independent from each other (due to the orthogonal conformation of the bridge), the predicted reduction or oxidation of the second subunit within a given homodyad is less favorable (min. ± 0.75 V). The only notable exception is the reduction of the second BNB-subunit of compound **2^{Mes}** (see Fig. S90†), which appears only −0.13 V more cathodically shifted than the first ($E_{2.red}$ = −2.68 V *vs.* $E_{1.red}$ = −2.55 V). This theoretical result again agrees well with the observation of the two partly resolved reduction waves at approx. −2.33 V in the CV of **2^{Mes}**.

The propensity of mixed (NBN,BNB)-dyads to experience charge-transfer (CT) transitions between the different heterocycles in the excited state was investigated by UV/vis absorption and emission spectroscopy. We first consider the three structurally closely related species **1^{Me}**, **2^{Me}**, and **3^{Me,Me}** in CH_2Cl_2 solutions (Fig. 3a and Table 1). As to be anticipated, no broad, bathochromic CT bands are visible in the absorption spectra of the two homodyads **1^{Me}** and **2^{Me}**. Moreover, either no (**1^{Me}**) or only very weak luminescence is detectable (**2^{Me}**; λ_{em} = 371 nm, Fig. 3b), suggesting that any local emission from the individual heterocyclic moieties can be neglected. Importantly, a switch from **2^{Me}** to **2^{Mes}** shifts the emission bathochromically (λ_{em} = 434 nm, Fig. 3b) and increases the fluorescence quantum yield by one order of magnitude (from Φ_{PL} = 2 to 22%; Table 1). According to quantum-chemical calculations (see below), the origin of this emission is mainly a CT from the mesityl substituents to the BNB-phenalenyl moiety.[12,27] The heterodyad **3^{Me,Me}** gives rise to a low-intensity absorption band between 400 and 550 nm that is most likely attributable to a CT transition from the NBN- to the BNB-phenalenyl fragment; **3^{Me,Me}** is non-emissive (see below for computed oscillator strengths and electron–hole plots).

To gain deeper insight into the low-lying excited states involved in absorption and emission, we performed time-dependent DFT (TD-DFT)[28] calculations in the Tamm-Dancoff approximation (TDA)[29] with the dispersion corrected,[16,30,31] optimally-tuned,[32–34] range-separated hybrid functional OT-LRC-ωPBEh-D4.[35,47,48] For vertical absorption energies

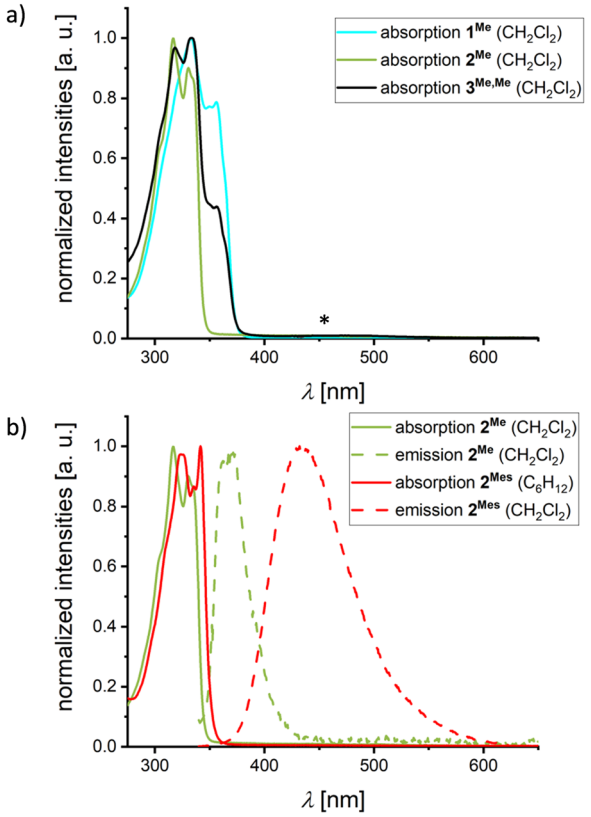

Fig. 3 (a) Normalized UV/vis absorption spectra of **1^{Me}**, **2^{Me}**, and **3^{Me,Me}** in CH_2Cl_2. The "*" symbol marks a low-intensity absorption maximum of **3^{Me,Me}** (an enlarged plot of this maximum is shown in Fig. S40†). (b) Normalized UV/vis absorption and emission spectra of **2^{Me}** (λ_{ex} = 330 nm) and **2^{Mes}** (λ_{ex} = 335 nm) in the specified solvents.

(E^c_{abs}), we combined TD-DFT with non-equilibrium perturbative ptSS-PCM[36,37] solvation (CH_2Cl_2) at the r2SCAN-3c/SMD optimized ground state geometries. Conversely, for vertical emission energies (E^c_{em}), we used iterative SS-PCM equilibrium solvation[38–40] at ΔSCF/UKS/PCM[41] optimized excited state geometries. This specific combination of ΔSCF/UKS and TD-DFT with continuum solvation mitigates some inherent shortcomings of TD-DFT for polar CT states in solution (see the ESI† for computational details).[12,42–44]

Due to their large oscillator strengths (f_{osc}), local excitations (LE) on one or both of the NBN/BNB-moieties are responsible for absorption. Moreover, the orthogonal arrangement of the NBN/BNB-fragments relative to the respective 1,4-phenylene bridge causes all intramolecular CT states to be dark (see the ESI† for a detailed discussion, including difference density plots and absorption energies calculated in different solvents). In the largely isostructural compounds **1^{Me}**, **2^{Me}**, and **3^{Me,Me}**, two states dominate the low-energy absorption: (i) a lower LE state on the NBN-fragments (**1^{Me}**/**3^{Me,Me}**; E^c_{abs} = 3.99 eV, f_{osc} = 0.052–0.104), and (ii) a strongly absorbing mixed LE state simultaneously on both NBN- and/or BNB-fragments (**1^{Me}**/**2^{Me}**/**3^{Me,Me}**; E^c_{abs} = 4.19 eV, f_{osc} = 0.672–0.705). The more hypsochromic onset of absorption observed for **2^{Me}** compared to

$\mathbf{1}^{\mathbf{Me}}$/$\mathbf{3}^{\mathbf{Me,Me}}$ is therefore likely attributable to the lack of an NBN moiety in $\mathbf{2}^{\mathbf{Me}}$ (see Fig. 3a).

Regarding the emission of $\mathbf{1}^{\mathbf{Me}}$, $\mathbf{2}^{\mathbf{Me}}$, and $\mathbf{3}^{\mathbf{Me,Me}}$, structural and solvent relaxation give rise to the following low-lying polar CT states (see Fig. 4): (i) a dark CT from the NBN-phenalenyl to the 1,4-phenylene bridge in $\mathbf{1}^{\mathbf{Me}}$ (E^{c}_{em} = 2.51 eV, f_{osc} = 0.008), (ii) a weakly allowed CT from the 1,4-phenylene bridge to the BNB unit in $\mathbf{2}^{\mathbf{Me}}$ (E^{c}_{em} = 2.85 eV, f_{osc} = 0.010), and (iii) a dipole-forbidden CT with vanishing transition density from the NBN to the BNB unit in $\mathbf{3}^{\mathbf{Me,Me}}$ (E^{c}_{em} = 1.68 eV, f_{osc} = 0.000). While the CT states of both type (i) and, in particular, type (iii) lie substantially below the respective LE (ΔE_{12} = 0.63 eV and 1.31 eV),[45] the gap for $\mathbf{2}^{\mathbf{Me}}$ is significantly smaller (0.38 eV). Considering the known artificial destabilization of LE states in NBN/BNB-phenalenyls by TD-DFT,[12] the state ordering of $\mathbf{2}^{\mathbf{Me}}$ falls within the error margins of our computational protocol. Consequently, $\mathbf{2}^{\mathbf{Me}}$ might retain some population for emission from the bright local S_2 state (*cf.* Fig. 3b and 4), while $\mathbf{1}^{\mathbf{Me}}$ and $\mathbf{3}^{\mathbf{Me,Me}}$ decay purely non-radiatively through the dark CT states.

The introduction of Mes substituents in $\mathbf{2}^{\mathbf{Mes}}$ lowers the CT state and increases its oscillator strength by mixing donor contributions from the 1,4-phenylene bridge and the Mes groups. Although the oscillator strength remains too low to significantly affect the absorption spectrum of $\mathbf{2}^{\mathbf{Mes}}$ (E^{c}_{abs} = 3.78 eV, f_{osc} = 0.010), relaxation of both the molecular structure in the excited state and the solvent shell leads the CT to be the relevant state for emission (E^{c}_{em} = 2.57 eV, f_{osc} = 0.019), which explains the broad, solvatochromically shifted band observed for $\mathbf{2}^{\mathbf{Mes}}$ (Fig. 3b and S36†).

Having studied the extent of *intra*molecular optoelectronic communication between the peripheral heterocycles in $\mathbf{1}^{\mathbf{Me}}$, $\mathbf{2}^{\mathbf{Me}}$, and $\mathbf{3}^{\mathbf{Me,Me}}$, the next step was to investigate possible *inter*molecular interactions. A viable method for producing the required intimately mixed aggregates is precipitation of the individual component molecules from THF by adding H_2O.[12] Since $\mathbf{3}^{\mathbf{Me,Me}}$ lacks long-term stability against hydrolysis, it was necessary to use its Mes-shielded derivative $\mathbf{3}^{\mathbf{Me,Mes}}$ instead. As a reference system, in which the 1,4-phenylene bridge is locked in a largely orthogonal conformation, $\mathbf{4}^{\mathbf{Me,Mes}}$ was also included in this study. In C_6H_{12} solution, $\mathbf{3}^{\mathbf{Me,Mes}}$ and $\mathbf{4}^{\mathbf{Me,Mes}}$ have emission maxima at 395 and 392 nm with Φ_{PL} values of 6 and 3%, respectively (Fig. 5a and S46;† Tables 1 and S1†); in THF, the quantum yields drop to 1 and 0%. Calculations confirm a weakly allowed Mes-to-BNB CT emission in C_6H_{12} (E^{c}_{em} = 3.60–3.64 eV, f_{osc} = 0.014–0.030). In polar solvents, a dipole-forbidden NBN-to-BNB CT state is dominant and effectively quenches any luminescence (E^{c}_{em} = 1.87–1.91 eV, f_{osc} = 0.000; in THF). Upon addition of H_2O to their THF solutions, the emission behavior of $\mathbf{3}^{\mathbf{Me,Mes}}$ and $\mathbf{4}^{\mathbf{Me,Mes}}$ changes dramatically: $\mathbf{3}^{\mathbf{Me,Mes}}$ shows a continuous decrease of the original blue emission[46] and a concomitant increase of a bathochromically shifted band at λ_{em} = 531 nm with Φ_{PL} = 6% (95% H_2O fraction, a further increase of the H_2O content lowers the emission intensity again; Fig. 5b). For $\mathbf{4}^{\mathbf{Me,Mes}}$ the aggregation-induced emission is even more pronounced with Φ_{PL} = 12% (λ_{em} =

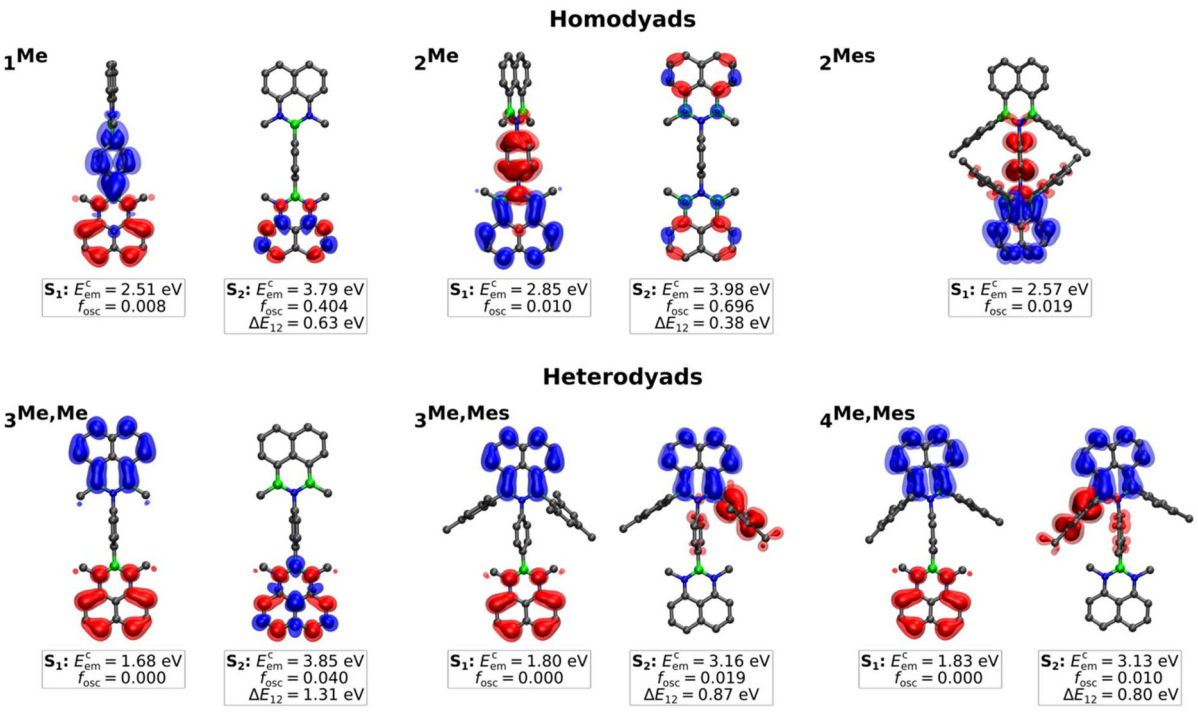

Fig. 4 Isosurface plots of the unrelaxed difference density (hole [red] and electron [blue]), calculated emission energies (E^{c}_{em}), and oscillator strengths (f_{osc}) in CH_2Cl_2 for the first two excited states of the homo- ($\mathbf{1}^{\mathbf{Me}}$, $\mathbf{2}^{\mathbf{Me}}$, $\mathbf{2}^{\mathbf{Mes}}$) and heterodyads ($\mathbf{3}^{\mathbf{Me,Me}}$, $\mathbf{3}^{\mathbf{Me,Mes}}$, $\mathbf{4}^{\mathbf{Me,Mes}}$) at the TDA-OT-LRC-ωPBEh-D4/def2-TZVPP/SS-PCM[CH_2Cl_2]//ΔSCF/UKS/PCM level of theory. 0.997 [opaque] and 0.999 [translucent] were used as isovalues.[45]

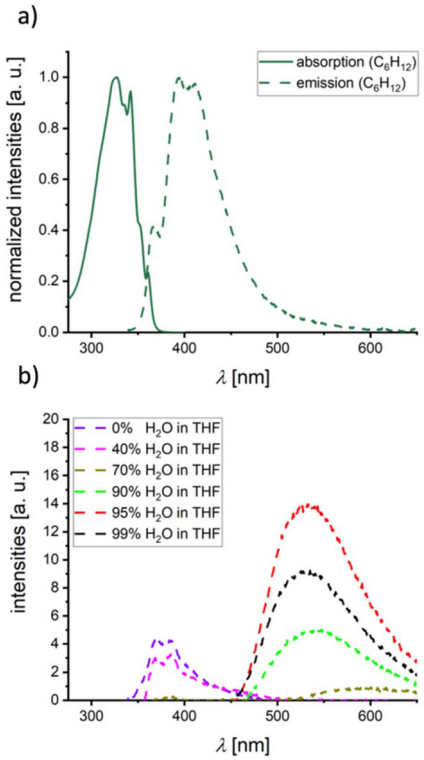

Fig. 5 (a) Normalized UV/vis absorption and emission spectra of $\mathbf{3}^{\mathbf{Me,Mes}}$ (C_6H_{12}, λ_{ex} = 327 nm). (b) Emission spectra of $\mathbf{3}^{\mathbf{Me,Mes}}$ (λ_{ex} = 327 nm) with differing H_2O fractions from 0% to 99% H_2O in THF. For the complete picture including all measured H_2O fractions, see Fig. S43 in the ESI.†

509 nm, 95% H_2O fraction; Fig. S47†). An in-depth quantum chemical investigation of *inter*molecular interactions in aggregates of $\mathbf{3}^{\mathbf{Me,Mes}}$ or $\mathbf{4}^{\mathbf{Me,Mes}}$ is not feasible due to prohibitively high computational costs. Instead, we have to refer to previous studies on *inter*molecular CT in mixtures of individual NBN- with BNB-phenalenyls, where the heteromolecular aggregates emit about 0.7 eV bathochromically shifted compared to the individual constituents. For $\mathbf{3}^{\mathbf{Me,Mes}}$, the energy difference between its emission in THF solution (λ_{em} = 370 nm) and in the aggregated state (λ_{em} = 531 nm) amounts to a similar value of 1.0 eV and can likely be traced back to head-to-tail aggregates of $\mathbf{3}^{\mathbf{Me,Mes}}$ resulting in *inter*molecular NBN-to-BNB CT.

Conclusions

NBN- and BNB-doped phenalenyls are isosters of phenalenyl anions and cations, respectively. Cyclic voltammetry on 1,4-phenylene-bridged $(NBN)_2$- or $(BNB)_2$-homodyads showed that this formal consideration is also relevant in practice, since the former are only oxidizable and the latter are only reducible within the THF solvent window. Remarkably, the NBN/BNB-heterodyad $\mathbf{4}^{\mathbf{Me,Mes}}$ undergoes both oxidation and reduction and can therefore be considered an ambipolar material. We have thus shown that the tool of heteroatom doping is suitable for generating (largely) isostructural species that still differ markedly in their electronic structures. Initially, we had hoped that the heterodyads would also show a bright intramolecular NBN-to-BNB charge-transfer emission. Yet, it turned out that the orthogonal conformation of the 1,4-phenylene linker prevents a pronounced interaction between the heterocyclic moieties and leads to a vanishing transition dipole. Aggregates of the heterodyads, however, show significant *inter*molecular CT emission, presumably due to head-to-tail alignment in the solid state. In order to also promote an intramolecular CT in the future, we are currently aiming to replace the 1,4-phenylene linker in the heterodyads with an 1,2-ethynediyl bridge.

Author contributions

A. S. synthesized and characterized all compounds. T. F. performed all quantum-chemical calculations. M. B. is responsible for the X-ray crystal structure analyses. H.-W. L., J.-M. M., and M. W. supervised the project. The manuscript was written by M. W., A. S., and T. F. and edited by all co-authors.

Conflicts of interest

There are no conflicts to declare.

Acknowledgements

T. F. thanks the Fonds der Chemischen Industrie (FCI) for funding through a Kekulé scholarship.

References

1 Q. Li, Y. Zhang, Z. Xie, Y. Zhen, W. Hu and H. Dong, Polycyclic aromatic hydrocarbon-based organic semiconductors: ring-closing synthesis and optoelectronic properties, *J. Mater. Chem. C*, 2022, **10**, 2411–2430.

2 For reviews regarding heteroatom doping, see: (*a*) Z. Liu and T. B. Marder, B–N versus C–C: How Similar Are They?, *Angew. Chem., Int. Ed.*, 2007, **47**, 242–244; (*b*) P. G. Campbell, A. J. V. Marwitz and S.-Y. Liu, Recent Advances in Azaborine Chemistry, *Angew. Chem., Int. Ed.*, 2012, **51**, 6074–6092; (*c*) G. Bélanger-Chabot, H. Braunschweig and D. K. Roy, Recent Developments in Azaborinine Chemistry, *Eur. J. Inorg. Chem.*, 2017, **2017**, 4353–4368; (*d*) E. von Grotthuss, A. John, T. Kaese and M. Wagner, Doping Polycyclic Aromatics with Boron for Superior Performance in Materials Science and Catalysis, *Asian J. Org. Chem.*, 2018, **7**, 37–53; (*e*) Z. X. Giustra and S.-Y. Liu, The State of the Art in Azaborine Chemistry: New Synthetic Methods and Applications, *J. Am. Chem. Soc.*, 2018, **140**, 1184–1194; (*f*) H. Helten, Doping the Backbone of π-Conjugated Polymers with Tricoordinate Boron: Synthetic Strategies and Emerging Applications, *Chem.* –

Asian J., 2019, **14**, 919–935; (*g*) X.-Y. Wang, X. Yao, A. Narita and K. Müllen, Heteroatom-Doped Nanographenes with Structural Precision, *Acc. Chem. Res.*, 2019, **52**, 2491–2505; (*h*) X. Chen, D. Tan and D.-T. Yang, Multiple-boron-nitrogen (multi-BN) doped π-conjugated systems for optoelectronics, *J. Mater. Chem. C*, 2022, **10**, 13499–13532.

3 For selected papers on B,N-PAHs, see: (*a*) A. J. V. Marwitz, M. H. Matus, L. N. Zakharov, D. A. Dixon and S.-Y. Liu, A Hybrid Organic/Inorganic Benzene, *Angew. Chem., Int. Ed.*, 2009, **48**, 973–977; (*b*) M. Krieg, F. Reicherter, P. Haiss, M. Ströbele, K. Eichele, M.-J. Treanor, R. Schaub and H. F. Bettinger, Construction of an Internally B_3N_3-Doped Nanographene Molecule, *Angew. Chem., Int. Ed.*, 2015, **54**, 8284–8286; (*c*) F.-D. Zhuang, J.-M. Han, S. Tang, J.-H. Yang, Q.-R. Chen, J.-Y. Wang and J. Pei, Efficient Modular Synthesis of Substituted Borazaronaphthalene, *Organometallics*, 2017, **36**, 2479–2482; (*d*) T. Kaehler, M. Bolte, H.-W. Lerner and M. Wagner, Introducing Perylene as a New Member to the Azaborine Family, *Angew. Chem., Int. Ed.*, 2019, **58**, 11379–11384; (*e*) M. Fingerle, S. Stocker and H. F. Bettinger, New Synthesis of a Dibenzoperylene Motif Featuring a Doubly Boron–Nitrogen-Doped Bay Region, *Synthesis*, 2019, **51**, 4147–4152; (*f*) K. Boknevitz, C. Darrigan, A. Chrostowska and S.-Y. Liu, Cation-π binding ability of BN indole, *Chem. Commun.*, 2020, **56**, 3749–3752; (*g*) M. Chen, K. S. Unikela, R. Ramalakshmi, B. Li, C. Darrigan, A. Chrostowska and S.-Y. Liu, A BN-Doped Cycloparaphenylene Debuts, *Angew. Chem., Int. Ed.*, 2021, **60**, 1556–1560; (*h*) O. Ouadoudi, T. Kaehler, M. Bolte, H.-W. Lerner and M. Wagner, One tool to bring them all: Au-catalyzed synthesis of B,O- and B,N-doped PAHs from boronic and borinic acids, *Chem. Sci.*, 2021, **12**, 5898–5909; (*i*) W. Li, C.-Z. Du, X.-Y. Chen, L. Fu, R.-R. Gao, Z.-F. Yao, J.-Y. Wang, W. Hu, J. Pei and X.-Y. Wang, BN–Anthracene for High–Mobility Organic Optoelectronic Materials through Periphery Engineering, *Angew. Chem., Int. Ed.*, 2022, **61**, e202201464.

4 J. Ahmed and S. K. Mandal, Phenalenyl Radical: Smallest Polycyclic Odd Alternant Hydrocarbon Present in the Graphene Sheet, *Chem. Rev.*, 2022, **122**, 11369–11431.

5 For papers regarding phenanyl radicals, see: (*a*) S. H. Glarum and J. H. Marshall, ESR of the Perinaphthenyl Radical in a Liquid Crystal, *J. Chem. Phys.*, 1966, **44**, 2884–2890; (*b*) K. Goto, T. Kubo, K. Yamamoto, K. Nakasuji, K. Sato, D. Shiomi, T. Takui, M. Kubota, T. Kobayashi, K. Yakusi and J. Ouyang, A Stable Neutral Hydrocarbon Radical: Synthesis, Crystal Structure, and Physical Properties of 2,5,8-Tri-tert-butyl-phenalenyl, *J. Am. Chem. Soc.*, 1999, **121**, 1619–1620; (*c*) Y. Morita, T. Ohba, N. Haneda, S. Maki, J. Kawai, K. Hatanaka, K. Sato, D. Shiomi, T. Takui and K. Nakasuji, New Persistent Radicals: Synthesis and Electronic Spin Structure of 2,5-Di-tert-butyl-6-Oxophenalenoxyl Derivatives, *J. Am. Chem. Soc.*, 2000, **122**, 4825–4826; (*d*) P. A. Koutentis, Y. Chen, Y. Cao, T. P. Best, M. E. Itkis, L. Beer, R. T. Oakley, A. W. Cordes, C. P. Brock and R. C. Haddon, Perchlorophenalenyl Radical, *J. Am. Chem. Soc.*, 2001, **123**, 3864–3871; (*e*) E. Turco, A. Bernhardt, N. Krane, L. Valenta, R. Fasel, M. Juríček and P. Ruffieux, Observation of the Magnetic Ground State of the Two Smallest Triangular Nanographenes, *JACS Au*, 2023, **3**, 1358–1364; (*f*) T. Kodama, Y. Hirao and T. Kubo, Synthesis and Properties of a Through-Space Interacting Diradicaloid, *Precis. Chem.*, 2023, **1**, 183–191.

6 For papers regarding phenalenyl anions, see: (*a*) V. Boekelheide and C. E. Larrabee, An Investigation of the Preparation and Some Properties of Perinaphthene, *J. Am. Chem. Soc.*, 1950, **72**, 1245–1249; (*b*) R. L. Shannon and R. H. Cox, On the alkali metal reduction of phenalene, *Tetrahedron Lett.*, 1973, **14**, 1603–1605.

7 For papers regarding phenalenyl cations, see: (*a*) R. Pettit, The Synthesis and Properties of the Perinaphthenylium Cation, *J. Am. Chem. Soc.*, 1960, **82**, 1972–1975; (*b*) A. Mukherjee, S. C. Sau and S. K. Mandal, Exploring Closed-Shell Cationic Phenalenyl: From Catalysis to Spin Electronics, *Acc. Chem. Res.*, 2017, **50**, 1679–1691; (*c*) T. Murata, K. Yoshida, S. Suzuki, A. Ueda, S. Nishida, J. Kawai, K. Fukui, K. Nakasuji and Y. Morita, Design and Synthesis of a C_3 Symmetrical Phenalenyl Derivative with Three Oxo Groups by Regioselective Deoxygenation/Oxygenation, *Org. Lett.*, 2022, **24**, 1033–1037.

8 For studies regarding NBN-phenalenyls, see: (*a*) Y. Lu, A. Bolag, J.-i. Nishida and Y. Yamashita, Synthesis and characterization of 1,3,2-diazaboroine derivatives for organic thin-film transistor applications, *Synth. Met.*, 2010, **160**, 1884–1891; (*b*) W.-M. Wan, D. Tian, Y.-N. Jing, X.-Y. Zhang, W. Wu, H. Ren and H.-L. Bao, NBN-Doped Conjugated Polycyclic Aromatic Hydrocarbons as an AIEgen Class for Extremely Sensitive Detection of Explosives, *Angew. Chem., Int. Ed.*, 2018, **57**, 15510–15516; (*c*) H. E. Hackney, M. Paladino, H. Fu and D. G. Hall, Diazaboryl-naphthyl-ketone: A New Scaffold with Bright Fluorescence, Aggregation-Induced Emission, and Application in the Quantitation of Trace Boronic Acids in Drug Intermediates, *Chem. – Eur. J.*, 2020, **26**, 14324–14329; (*d*) Y. Zeng, J. Yang and X. Zheng, Aggregation effects on photophysical properties of NBN-doped polycyclic aromatic hydrocarbons: a theoretical study, *Phys. Chem. Chem. Phys.*, 2021, **23**, 23986–23997.

9 For examples of π-extended NBN-aromatics, see: (*a*) M. Numano, N. Nagami, S. Nakatsuka, T. Katayama, K. Nakajima, S. Tatsumi, N. Yasuda and T. Hatakeyama, Synthesis of Boronate-Based Benzo[*fg*]tetracene and Benzo[*hi*]hexacene via Demethylative Direct Borylation, *Chem. – Eur. J.*, 2016, **22**, 11574–11577; (*b*) X. Wang, F. Zhang, K. S. Schellhammer, P. Machata, F. Ortmann, G. Cuniberti, Y. Fu, J. Hunger, R. Tang, A. A. Popov, R. Berger, K. Müllen and X. Feng, Synthesis of NBN-Type Zigzag-Edged Polycyclic Aromatic Hydrocarbons: 1,9-Diaza-9a-boraphenalene as a Structural Motif, *J. Am. Chem. Soc.*, 2016, **138**, 11606–11615; (*c*) D.-T. Yang, T. Nakamura, Z. He, X. Wang, A. Wakamiya, T. Peng and S. Wang, Doping Polycyclic

Arenes with Nitrogen–Boron–Nitrogen (NBN) Units, *Org. Lett.*, 2018, **20**, 6741–6745; (*d*) Y. Fu, K. Zhang, E. Dmitrieva, F. Liu, J. Ma, J. J. Weigand, A. A. Popov, R. Berger, W. Pisula, J. Liu and X. Feng, NBN-embedded Polycyclic Aromatic Hydrocarbons Containing Pentagonal and Heptagonal Rings, *Org. Lett.*, 2019, **21**, 1354–1358; (*e*) P. Qiang, Z. Sun, M. Wan, X. Wang, P. Thiruvengadam, C. Bingi, W. Wei, W. Zhu, D. Wu and F. Zhang, Successive Annulation to Fully Zigzag-Edged Polycyclic Heteroaromatic Hydrocarbons with Strong Blue–Green Electroluminescence, *Org. Lett.*, 2019, **21**, 4575–4579; (*f*) C.-W. Ju, B. Li, L. Li, W. Yan, C. Cui, X. Ma and D. Zhao, Modular Synthesis of Pentagonal and Hexagonal Ring-Fused NBN-Phenalenes Leading to an Excited-State Aromatization-Induced Structural Planarization Molecular Library, *J. Am. Chem. Soc.*, 2021, **143**, 5903–5916; (*g*) M. Zhao and Q. Miao, Design, Synthesis and Hydrogen Bonding of B_3N_6-[4]Triangulene, *Angew. Chem., Int. Ed.*, 2021, **60**, 21289–21294; (*h*) M. Franceschini, M. Crosta, R. R. Ferreira, D. Poletto, N. Demitri, J. P. Zobel, L. González and D. Bonifazi, Peri-Acenoacene Ribbons with Zigzag BN-Doped Peripheries, *J. Am. Chem. Soc.*, 2022, **144**, 21470–21484.

10 A. S. Scholz, J. G. Massoth, M. Bursch, J.-M. Mewes, T. Hetzke, B. Wolf, M. Bolte, H.-W. Lerner, S. Grimme and M. Wagner, BNB-Doped Phenalenyls: Modular Synthesis, Optoelectronic Properties, and One-Electron Reduction, *J. Am. Chem. Soc.*, 2020, **142**, 11072–11083.

11 Examples of BNB-phenalenyls: (*a*) H. Wei, Y. Liu, T. Y. Gopalakrishna, H. Phan, X. Huang, L. Bao, J. Guo, J. Zhou, S. Luo, J. Wu and Z. Zeng, B–N–B Bond Embedded Phenalenyl and Its Anions, *J. Am. Chem. Soc.*, 2017, **139**, 15760–15767; (*b*) M. Crumbach, O. Ayhan, L. Fritze, J. A. P. Sprenger, L. Zapf, M. Finze and H. Helten, BNB-doped phenalenyls - aromaticity switch upon one-electron reduction, *Chem. Commun.*, 2021, **57**, 2408–2411. For references regarding π-extended or related systems, see: (*c*) M. Fingerle, C. Maichle-Mössmer, S. Schundelmeier, B. Speiser and H. F. Bettinger, Synthesis and Characterization of a Boron–Nitrogen–Boron Zigzag-Edged Benzo[*fg*]tetracene Motif, *Org. Lett.*, 2017, **19**, 4428–4431; (*d*) M. Crumbach, J. Bachmann, L. Fritze, A. Helbig, I. Krummenacher, H. Braunschweig and H. Helten, Dithiophene-Fused Oxadiborepins and Azadiborepins: A New Class of Highly Fluorescent Heteroaromatics, *Angew. Chem., Int. Ed.*, 2021, **60**, 9290–9295; (*e*) J. Bachmann, A. Helbig, M. Crumbach, I. Krummenacher, H. Braunschweig and H. Helten, Fusion of Aza- and Oxadiborepins with Furans in a Reversible Ring-Opening Process Furnishes Versatile Building Blocks for Extended π-Conjugated Materials, *Chem. – Eur. J.*, 2022, **28**, e202202455; (*f*) T. Bischof, L. Beßler, I. Krummenacher, L. Erhard, H. Braunschweig and M. Finze, Construction of a Diverse Range of Boron Heterocycles via Ring Expansion of a Carboranyl–Substituted 9-Borafluorene, *Chem. – Eur. J.*, 2023, **29**, e202300210; (*g*) S. Zhou, Y. Liu, W. Jin, T. Qin, X. Liu, C. Zhao, Z. Liu and X. Yu, Synthesis, Structures, and Photophysical Properties of Zigzag BNBNB-Embedded Anthracene-Fused Fluoranthene, *Org. Lett.*, 2023, **25**, 1573–1577.

12 A. S. Scholz, J. G. Massoth, L. Stoess, M. Bolte, M. Braun, H.-W. Lerner, J.-M. Mewes, M. Wagner and T. Froitzheim, NBN- and BNB-Phenalenyls: the Yin and Yang of Heteroatom-doped π Systems, *Chem. – Eur. J.*, 2024, e202400320.

13 (*a*) F. F. Caserio Jr., J. J. Cavallo and R. I. Wagner, Preparation of 8-Bora-7,9-diazaro-peri-naphthene and Derivatives, *J. Org. Chem.*, 1961, **26**, 2157–2158; (*b*) V. M. Jiménez-Pérez, B. M. Muñoz-Flores, H. W. Roesky, T. Schulz, A. Pal, T. Beck, Z. Yang, D. Stalke, R. Santillan and M. Witt, Monomeric Boron and Tin(II) Heterocyclic Derivatives of 1,8-Diaminonaphthalenes: Synthesis, Characterization and X-ray Structures, *Eur. J. Inorg. Chem.*, 2008, **2008**, 2238–2243.

14 M. Karplus and J. A. Pople, Theory of Carbon NMR Chemical Shifts in Conjugated Molecules, *J. Chem. Phys.*, 1963, **38**, 2803–2807.

15 Y.-S. Lin, G.-D. Li, S.-P. Mao and J.-D. Chai, Long-Range Corrected Hybrid Density Functionals with Improved Dispersion Corrections, *J. Chem. Theory Comput.*, 2013, **9**, 263–272.

16 S. Grimme, A. Hansen, J. G. Brandenburg and C. Bannwarth, Dispersion-Corrected Mean-Field Electronic Structure Methods, *Chem. Rev.*, 2016, **116**, 5105–5154.

17 J. Zheng, X. Xu and D. G. Truhlar, Minimally augmented Karlsruhe basis sets, *Theor. Chem. Acc.*, 2011, **128**, 295–305.

18 F. Weigend and R. Ahlrichs, Balanced basis sets of split valence, triple zeta valence and quadruple zeta valence quality for H to Rn: Design and assessment of accuracy, *Phys. Chem. Chem. Phys.*, 2005, **7**, 3297–3305.

19 F. Weigend, Accurate Coulomb-fitting basis sets for H to Rn, *Phys. Chem. Chem. Phys.*, 2006, **8**, 1057–1065.

20 A. V. Marenich, C. J. Cramer and D. G. Truhlar, Universal Solvation Model Based on Solute Electron Density and on a Continuum Model of the Solvent Defined by the Bulk Dielectric Constant and Atomic Surface Tensions, *J. Phys. Chem. B*, 2009, **113**, 6378–6396.

21 P. Winget, D. M. Dolney, D. J. Giesen, C. J. Cramer and D. G. Truhlar, Minnesota Solvent Descriptor Database, **https://comp.chem.umn.edu/solvation/**, (accessed 4 March 2024).

22 S. Grimme, J. Antony, S. Ehrlich and H. Krieg, A consistent and accurate ab initio parametrization of density functional dispersion correction (DFT-D) for the 94 elements H-Pu, *J. Chem. Phys.*, 2010, **132**, 154104.

23 S. Grimme, A. Hansen, S. Ehlert and J.-M. Mewes, r^2SCAN-3c: A "Swiss army knife" composite electronic-structure method, *J. Chem. Phys.*, 2021, **154**, 064103.

24 A. V. Marenich, C. P. Kelly, J. D. Thompson, G. D. Hawkins, C. C. Chambers, D. J. Giesen, P. Winget, C. J. Cramer and D. G. Truhlar, Minnesota Solvation Database (MNSOL) version 2012, **https://doi.org/10.13020/3eks-j059**, (accessed 5 March 2024).

25 D. L. Mobley and J. P. Guthrie, FreeSolv: a database of experimental and calculated hydration free energies, with input files, *J. Comput.-Aided Mol. Des*, 2014, **28**, 711–720.
26 C. Plett, M. Stahn, M. Bursch, J.-M. Mewes and S. Grimme, Improving Quantum Chemical Solvation Models by Dynamic Radii Adjustment for Continuum Solvation (DRACO), *J. Phys. Chem. Lett.*, 2024, **15**, 2462–2469.
27 This interpretation is in line with a continuous bathochromic shift of the emission band upon increasing the solvent polarity from C_6H_{12} (λ_{em} = 399 nm) to C_6H_6 (408 nm), THF (421 nm), and CH_2Cl_2 (434 nm, Fig. S36†).
28 E. Runge and E. K. U. Gross, Density-Functional Theory for Time-Dependent Systems, *Phys. Rev. Lett.*, 1984, **52**, 997–1000.
29 S. Hirata and M. Head-Gordon, Time-dependent density functional theory within the Tamm–Dancoff approximation, *Chem. Phys. Lett.*, 1999, **314**, 291–299.
30 E. Caldeweyher, C. Bannwarth and S. Grimme, Extension of the D3 dispersion coefficient model, *J. Chem. Phys.*, 2017, **147**, 034112.
31 E. Caldeweyher, S. Ehlert, A. Hansen, H. Neugebauer, S. Spicher, C. Bannwarth and S. Grimme, A generally applicable atomic-charge dependent London dispersion correction, *J. Chem. Phys.*, 2019, **150**, 154122.
32 T. Stein, L. Kronik and R. Baer, Prediction of charge-transfer excitations in coumarin-based dyes using a range-separated functional tuned from first principles, *J. Chem. Phys.*, 2009, **131**, 244119.
33 R. Baer, E. Livshits and U. Salzner, Tuned Range-Separated Hybrids in Density Functional Theory, *Annu. Rev. Phys. Chem.*, 2010, **61**, 85–109.
34 J. Shee and M. Head-Gordon, Predicting Excitation Energies of Twisted Intramolecular Charge-Transfer States with the Time-Dependent Density Functional Theory: Comparison with Experimental Measurements in the Gas Phase and Solvents Ranging from Hexanes to Acetonitrile, *J. Chem. Theory Comput.*, 2020, **16**, 6244–6255.
35 M. A. Rohrdanz, K. M. Martins and J. M. Herbert, A long-range-corrected density functional that performs well for both ground-state properties and time-dependent density functional theory excitation energies, including charge-transfer excited states, *J. Chem. Phys.*, 2009, **130**, 054112.
36 J.-M. Mewes, Z.-Q. You, M. Wormit, T. Kriesche, J. M. Herbert and A. Dreuw, Experimental Benchmark Data and Systematic Evaluation of Two a Posteriori, Polarizable-Continuum Corrections for Vertical Excitation Energies in Solution, *J. Phys. Chem. A*, 2015, **119**, 5446–5464.
37 S. Chibani, Š. Budzák, M. Medved', B. Mennucci and D. Jacquemin, Full cLR-PCM calculations of the solvatochromic effects on emission energies, *Phys. Chem. Chem. Phys.*, 2014, **16**, 26024–26029.
38 J. M. Herbert, Dielectric continuum methods for quantum chemistry, *Wiley Interdiscip. Rev.: Comput. Mol. Sci.*, 2021, **11**, e1519.
39 R. Improta, V. Barone, G. Scalmani and M. J. Frisch, A state-specific polarizable continuum model time dependent density functional theory method for excited state calculations in solution, *J. Chem. Phys.*, 2006, **125**, 054103.
40 J.-M. Mewes, J. M. Herbert and A. Dreuw, On the accuracy of the general, state-specific polarizable-continuum model for the description of correlated ground- and excited states in solution, *Phys. Chem. Chem. Phys.*, 2017, **19**, 1644–1654.
41 A. T. B. Gilbert, N. A. Besley and P. M. W. Gill, Self-Consistent Field Calculations of Excited States Using the Maximum Overlap Method (MOM), *J. Phys. Chem. A*, 2008, **112**, 13164–13171.
42 T. Froitzheim, S. Grimme and J.-M. Mewes, Either Accurate Singlet–Triplet Gaps or Excited-State Structures: Testing and Understanding the Performance of TD-DFT for TADF Emitters, *J. Chem. Theory Comput.*, 2022, **18**, 7702–7713.
43 L. Kunze, A. Hansen, S. Grimme and J.-M. Mewes, PCM-ROKS for the Description of Charge-Transfer States in Solution: Singlet–Triplet Gaps with Chemical Accuracy from Open-Shell Kohn–Sham Reaction-Field Calculations, *J. Phys. Chem. Lett.*, 2021, **12**, 8470–8480.
44 J.-M. Mewes, Modeling TADF in organic emitters requires a careful consideration of the environment and going beyond the Franck–Condon approximation, *Phys. Chem. Chem. Phys.*, 2018, **20**, 12454–12469.
45 ΔE_{12} is the energy difference between the first and second excited states with fully relaxed equilibrium solvation at their respective ΔSCF/UKS/PCM geometries. Due to the differences in structure and solvent environment, ΔE_{12} deviates substantially from the difference of either emission or absorption energies.
46 The emission maximum of $\mathbf{3^{Me,Mes}}$ in pure THF is λ_{em} = 389 nm at a concentration of 1.5×10^{-5} mol L^{-1}; the mixtures used for the H_2O-precipitation studies had a higher concentration of 1.5×10^{-4} mol L^{-1} and gave a λ_{em} of 370 nm. The origin of this slight hypsochromic shift is unknown.
47 E. Epifanovsky, A. T. B. Gilbert, X. Feng, J. Lee, Y. Mao, N. Mardirossian, P. Pokhilko, A. F. White, M. P. Coons, A. L. Dempwolff, Z. Gan, D. Hait, P. R. Horn, L. D. Jacobson, I. Kaliman, J. Kussmann, A. W. Lange, K. U. Lao, D. S. Levine, J. Liu, S. C. McKenzie, A. F. Morrison, K. D. Nanda, F. Plasser, D. R. Rehn, M. L. Vidal, Z.-Q. You, Y. Zhu, B. Alam, B. J. Albrecht, A. Aldossary, E. Alguire, J. H. Andersen, V. Athavale, D. Barton, K. Begam, A. Behn, N. Bellonzi, Y. A. Bernard, E. J. Berquist, H. G. A. Burton, A. Carreras, K. Carter-Fenk, R. Chakraborty, A. D. Chien, K. D. Closser, V. Cofer-Shabica, S. Dasgupta, M. de Wergifosse, J. Deng, M. Diedenhofen, H. Do, S. Ehlert, P.-T. Fang, S. Fatehi, Q. Feng, T. Friedhoff, J. Gayvert, Q. Ge, G. Gidofalvi, M. Goldey, J. Gomes, C. E. González-Espinoza, S. Gulania, A. O. Gunina, M. W. D. Hanson-Heine, P. H. P. Harbach, A. Hauser, M. F. Herbst, M. Hernández Vera, M. Hodecker, Z. C. Holden, S. Houck, X. Huang, K. Hui, B. C. Huynh, M. Ivanov, Á. Jász, H. Ji, H. Jiang, B. Kaduk, S. Kähler, K. Khistyaev, J. Kim, G. Kis, P. Klunzinger, Z. Koczor-Benda, J. H. Koh, D. Kosenkov, L. Koulias, T. Kowalczyk,

C. M. Krauter, K. Kue, A. Kunitsa, T. Kus, I. Ladjánszki, A. Landau, K. V. Lawler, D. Lefrancois, S. Lehtola, R. R. Li, Y.-P. Li, J. Liang, M. Liebenthal, H.-H. Lin, Y.-S. Lin, F. Liu, K.-Y. Liu, M. Loipersberger, A. Luenser, A. Manjanath, P. Manohar, E. Mansoor, S. F. Manzer, S.-P. Mao, A. V. Marenich, T. Markovich, S. Mason, S. A. Maurer, P. F. McLaughlin, M. F. S. J. Menger, J.-M. Mewes, S. A. Mewes, P. Morgante, J. W. Mullinax, K. J. Oosterbaan, G. Paran, A. C. Paul, S. K. Paul, F. Pavošević, Z. Pei, S. Prager, E. I. Proynov, Á. Rák, E. Ramos-Cordoba, B. Rana, A. E. Rask, A. Rettig, R. M. Richard, F. Rob, E. Rossomme, T. Scheele, M. Scheurer, M. Schneider, N. Sergueev, S. M. Sharada, W. Skomorowski, D. W. Small, C. J. Stein, Y.-C. Su, E. J. Sundstrom, Z. Tao, J. Thirman, G. J. Tornai, T. Tsuchimochi, N. M. Tubman, S. P. Veccham, O. Vydrov, J. Wenzel, J. Witte, A. Yamada, K. Yao, S. Yeganeh, S. R. Yost, A. Zech, I. Y. Zhang, X. Zhang, Y. Zhang, D. Zuev, A. Aspuru-Guzik, A. T. Bell, N. A. Besley, K. B. Bravaya, B. R. Brooks, D. Casanova, J.-D. Chai, S. Coriani, C. J. Cramer, G. Cserey, A. E. DePrince III, R. A. DiStasio Jr., A. Dreuw, B. D. Dunietz, T. R. Furlani, W. A. Goddard III, S. Hammes-Schiffer, T. Head-Gordon, W. J. Hehre, C.-P. Hsu, T.-C. Jagau, Y. Jung, A. Klamt, J. Kong, D. S. Lambrecht, W. Liang, N. J. Mayhall, C. W. McCurdy, J. B. Neaton, C. Ochsenfeld, J. A. Parkhill, R. Peverati, V. A. Rassolov, Y. Shao, L. V. Slipchenko, T. Stauch, R. P. Steele, J. E. Subotnik, A. J. W. Thom, A. Tkatchenko, D. G. Truhlar, T. Van Voorhis, T. A. Wesolowski, K. B. Whaley, H. L. Woodcock III, P. M. Zimmerman, S. Faraji, P. M. W. Gill, M. Head-Gordon, J. M. Herbert and A. I. Krylov, Software for the frontiers of quantum chemistry: An overview of developments in the Q-Chem 5 package, *J. Chem. Phys.*, 2021, **155**, 084801.

48 F. Neese, The ORCA program system, *Wiley Interdiscip. Rev.: Comput. Mol. Sci.*, 2012, **2**, 73–78.